Journal of Materials Chemistry A

Accepted Manuscript

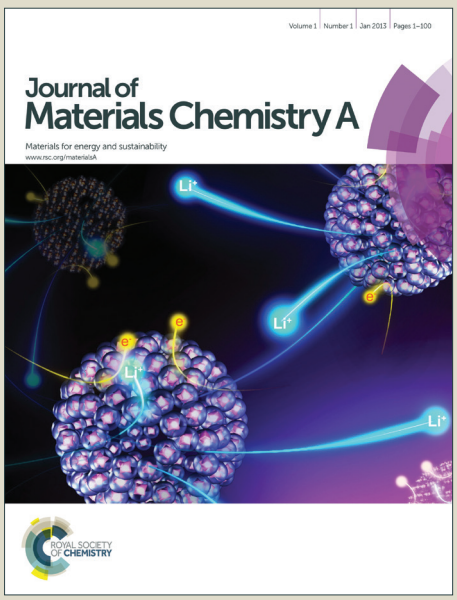

ROYAL SOCIETY OF CHEMISTRY

www.rsc.org/materialsA

Ultrathin $NiCo_2O_4$ nanosheets grown on three-dimensional interwoven nitrogen-doped carbon nanotubes as binder-free electrodes for high-performance supercapacitors

Jian Wu[a,b], Pan Guo[a], Rui Mi[b], Xichuan Liu[b], Hui Zhang[b], Jun Mei[b], Hao Liu[*,b], Woon-Ming Lau[a,b], Li-Min Liu[*,a]

[a]*Beijing Computational Science Research Center, Beijing 100084, China*
[b]*Chengdu Green Energy and Green Manufacturing Technology R&D Center, Chengdu Development Center of Science and Technology of CAEP, Chengdu, Sichuan, 610207, China*

*Corresponding authors (Hao Liu and Li-Min Liu)

E-mail: mliuhao@gmail.com; Tel.: 0086-28-67076208.

E-mail: limin.liu@csrc.ac.cn; Tel.: 0086-10-82687086.

Abstract

A novel three-dimensional (3D) Ni foam/N-CNTs/$NiCo_2O_4$ nanosheets electrode was synthesized by combining a chemical vapor deposition method and a facile electrochemical deposition method followed by a calcination process. The N-CNTs entangle each other and construct a 3D highly conductive network, creating a structure which offers a skeleton for homogeneous electrodeposition of thin $NiCo_2O_4$ nanosheets. By taking advantage of the one-dimensional (1D) N-CNTs, the two-dimensional (2D) ultrathin nanosheets and the 3D hybrid structure, the 3D Ni foam/N-CNTs/$NiCo_2O_4$ nanosheets electrode exhibits superior supercapacitive performances with high specific capacitance (1472 F g^{-1} at 1 A g^{-1}), remarkable rate capability and excellent cycling stability (less than 1% loss after 3000 cycles). The

outstanding supercapacitive performance is attributed to the highly conductive 3D Ni foam/N-CNTs substrates and the ultrathin morphology of the $NiCo_2O_4$ nanosheets. The former offers a strong skeleton for uniform electrodeposition, endures the volume change, and provides a good electrical conducting pathway for ion and electron transport; meanwhile the latter possesses numerous active sites and short diffusion path. Moreover, the synthesis strategy can be extended to the preparation of other 3D electrode materials for supercapacitors and other energy-storage devices.

Introduction

The impending energy crisis and the environmental pollution have triggered tremendous research into the design and development of various types of advanced energy storage devices.[1-3] Supercapacitors are practical and environmentally friendly energy storage devices with high power density, long cycling stability, fast deliver rate and improved safety.[4-7] Pseudocapacitors, as one of the two types of supercapacitors, possess a higher capacitance than the other (electrical double-layer capacitors) due to their fast faradaic reactions on the electrode surface.[8-10]

Among various pseudocapacitor materials, spinel nickel cobaltite ($NiCo_2O_4$) has attracted intense attention owing to its high theoretical capacitance, rich redox reactions, low cost and environmental friendliness.[11-14] However, the self-assembled $NiCo_2O_4$ materials (grown without substrate) usually suffer from low capacitance, poor rate performance and short cycle life due to structural instability and insufficient

utilization of active materials.[15-17] Therefore, in order to improve the utilization rate of active materials and enhance their electrochemical performance, rational design of electroactive materials directly on 3D conductive substrates (such as carbon fiber,[18] Ni foam,[19] graphene,[20] stainless-steel foil[21] *etc*.) or a hierarchical core-shell structure (such as $NiCo_2O_4@Co_xNi_{1-x}(OH)_2$,[22] $NiCo_2O_4@MnO_2$,[23] $Co_3O_4@Pt@MnO_2$,[24] *etc*.) have attracted extensive attention. Moreover, without the use of any polymer binder, these binder-free supercapacitor electrodes show dramatically enhanced electrochemical performance due to the increased active surface area and the enhanced ion diffusion and electronic conductivity.[10, 25]

Recently, nitrogen-doped carbon materials (such as N-graphene, N-CNTs and N-carbon xerogels, N-doped mesoporous carbon *etc*.) and their hybrid nanocomposites have been widely utilized in supercapacitors, water oxidation, electrochemical biosensing and lithium-ion batteries *etc*.[26-30] Both theoretical and experimental results confirm that the application of nitrogen-doped carbon materials can not only immobilize their surface metal particles, but also act synergistically and improve the electrochemical activity of the hybrid nanocomposites.[31-36] Especially, the 1D N-CNTs show great electron mobility, and can offer a strong skeleton for homogeneous growth of active materials.[37, 38] On the other hand, among numerous nanostructures, 2D nanosheets (NS), especially those with the ultrathin morphology and interconnected structure, exhibit remarkable electrochemical performance because of their fast ion/electron transport, better accommodation of volume expansion and large surface area.[39-42] Based on all these findings, it is speculated that

a hybrid electrode using directly grown electrode materials on the 1D N-CNTs with a 2D ultrathin nanosheets nanostructure could possess remarkable electrochemical performances due to the above merits.

In this study, nitrogen-doped carbon nanotubes (N-CNTs) are prepared on nickel foam by a chemical vapor deposition method and interwoven with each other to form a 3D conducting network. Ultrathin $NiCo_2O_4$ nanosheets were then homogeneously grown on this N-CNTs based skeleton by electrodeposition. Results show that when used as binder-free supercapacitor electrodes, the 3D Ni foam/N-CNTs/$NiCo_2O_4$ nanosheets structure exhibits superior supercapacitive performances. The specific capacitance is 1472 F g^{-1} at the current density of 1 A g^{-1}, the rate capability is 73% retention as the current density increased to 30 A g^{-1}, and the cycling durability is more than 99% retention over 3000 cycles at the current density of 10 A g^{-1} and 81% retention after 9000 cycles at the current density of 20 A g^{-1}. The 3D hybrid electrode structure can be integrated into other energy-storage devices.

Experimental

Preparation of N-CNTs on Ni foam

N-CNTs were grown on Ni foam via a chemical vapor deposition (CVD) method, as reported in our previous work.[43, 44] Briefly, the circular Ni foam with a diameter of 16 mm was ultrasonically cleaned in 2 M HCl solution for 20 min, and then rinsed with deionized water (DI) and ethanol extensively. Subsequently, the prepared Ni foam as the substrate to grow N-CNTs was placed into a quartz tube. Ferrocene, ethylene gas and melamine were employed as the catalyst, the carbon source and the

nitrogen source, respectively.

Preparation of 3D Ni foam/N-CNTs/$NiCo_2O_4$ nanosheets

For the preparation of ultrathin $NiCo_2O_4$ nanosheets directly on the 3D Ni foam/N-CNTs, a simple electrodeposition was employed in a three-electrode system with the 3D Ni foam/N-CNTs as the working electrode, a platinum foil as the counter electrode and a saturated calomel electrode (SCE) as the reference electrode. The Co-Ni bimetallic hydroxides were electrodeposited on the as-prepared substrates in an aqueous electrolyte with 4 mmol $Co(NO_3)_2 \cdot 6H_2O$ and 2 mmol $Ni(NO_3)_2 \cdot 6H_2O$ at a constant cathodic current of 1 mA cm^{-2} for 10 min at room temperature. After electrodeposition, the as-prepared sample was washed several times with DI water, and then dried at 60 ℃ for 12 h. Finally, the sample was annealed at 300 ℃ in air for 2 h with a ramp rate of 1 ℃ min^{-1}. The $NiCo_2O_4$ nanosheets were obtained and, using a high precision electronic balance, the active mass loading is measured to be about 0.50 mg cm^{-2} on average. For comparison, $NiCo_2O_4$ nanosheets on Ni foam were also synthesized in the same way with the Ni foam as the working electrode and the active mass loading is also about 0.50 mg cm^{-2}.

Material characterization

The crystallographic structures of the product were obtained from X-ray diffraction (XRD, D/max 2200/PC, Rigaku, 40 kV, 20 mA, Cu K_α radiation, λ = 1.5406 Å). The morphology and elemental information of the sample were investigated by a scanning electron microscopy (SEM, Hitachi S-5200) equipped with an energy dispersive X-ray spectrometer (EDX). The microstructure of the material

was carried out by a transmission electron microscope (TEM, JEOL JEM-2010). The surface area was determined by Brunauer-Emmett-Teller (BET) nitrogen adsorption-desorption. (Autosorb-iQ)

Electrochemical measurements

All electrochemical measurements were performed using a CHI760E electrochemical workstation at room temperature in the 2M KOH aqueous electrolyte. A three-electrode system was employed to measure the response of the Ni foam/ $NiCo_2O_4$ nanosheets electrode and the 3D Ni foam/N-CNTs/$NiCo_2O_4$ nanosheets electrode as the working electrode, with a slice of Pt foil as the counter electrode and a standard Hg/HgO electrode as the reference electrode. The cyclic voltammetry (CV) measurements were carried out at various scan rates between 0- 0.75 V (*vs*. Hg/HgO). The charge-discharge tests were measured with the potential window from 0 to 0.55 V (*vs*. Hg/HgO) at different current densities. The electrochemical impedance spectroscopy (EIS) plots were done over the frequency range of 100 kHz to 0.01 Hz with an amplitude of 5 mV. The capacitance (*C*), specific energy density (*E*) and power density (*P*) were calculated respectively by,[45, 46]

$$C = \frac{I\Delta t}{S\Delta V} \text{ or } C = \frac{I\Delta t}{m\Delta V} \quad (1)$$

$$E = \frac{1}{2} C\Delta V^2 \quad (2)$$

$$P = \frac{E}{\Delta t} \quad (3)$$

where I (A) is the discharge current, Δt (s) is the discharge time, ΔV (V) is the potential window of discharge, S (cm^2) is the area of the working electrode, m (g) is the mass of the active material

Results and discussion

Structure and Morphology

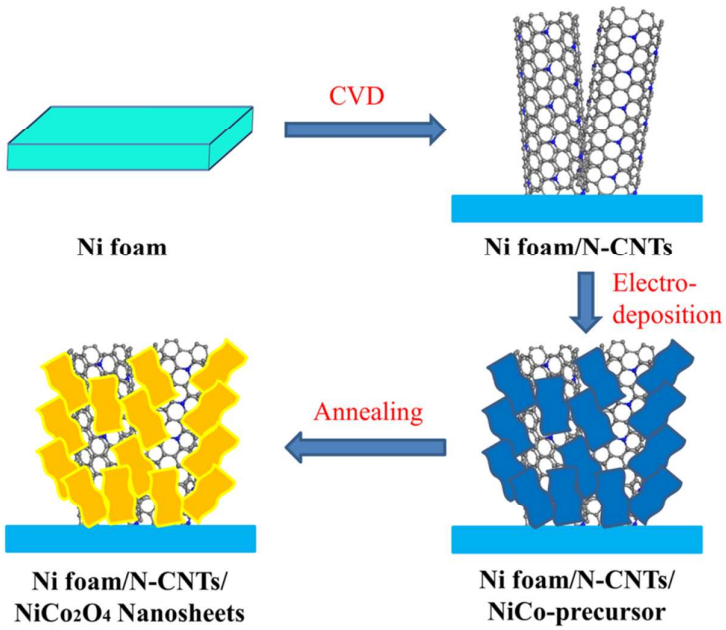

Fig. 1 Schematic diagram of the fabrication process of ultrathin $NiCo_2O_4$ nanosheets on nickel foam substrate-supported 3D interweaved nitrogen-doped carbon nanotubes.

The synthesis procedure of the 3D Ni foam/N-CNTs/$NiCo_2O_4$ NS is schematically illustrated in **Fig. 1**. Firstly, N-doped carbon nanotubes are synthesized via a one-step CVD method on Ni foam. Subsequently, a simple and effective co-electrodeposition method introduces the Ni-Co layered hydroxide precursor on the N-CNTs. In the electrodeposition process, the electrochemical reactions are illustrated by the following equations:[41, 47]

$$NO_3^- + H_2O + 2e^- \rightarrow NO_2^- + 2OH^- \quad (4)$$

$$NO_3^- + 6H_2O + 6e^- \rightarrow NH_4^+ + 8OH^- \quad (5)$$

$$xNi^{2+} + 2xCo^{2+} + 6xOH^- \rightarrow Ni_xCo_{2x}(OH)_{6x} \quad (6)$$

Finally, the Ni-Co bimetallic hydroxide precursor is converted to the spinel $NiCo_2O_4$ by a simple thermal treatment in air:[41, 47]

$$Ni_xCo_{2x}(OH)_{6x} + \frac{1}{2}xO_2 \rightarrow \ xNiCo_2O_4 + \ 3xH_2O \qquad (7)$$

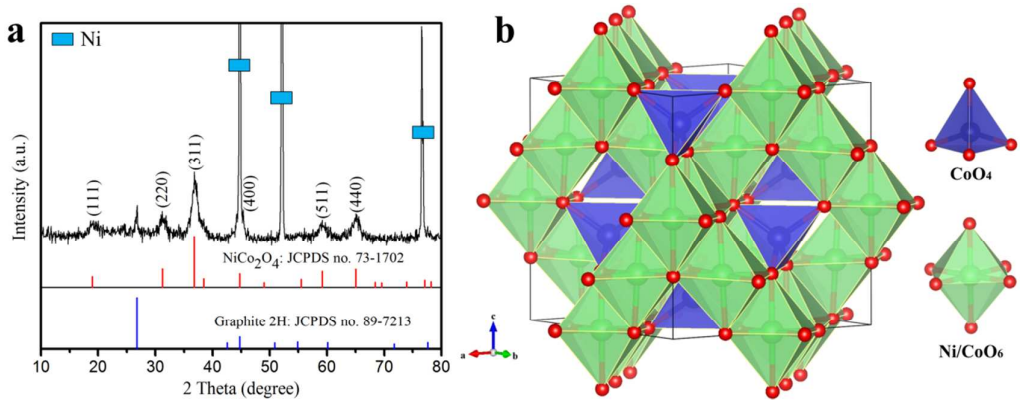

Fig. 2 (a) Typical XRD pattern of the Ni foam/N-CNTs/$NiCo_2O_4$ NS; (b) crystal structure of $NiCo_2O_4$ cubic spinel (ICSD No.02241).

The crystallographic structure and phase purity of the as-prepared product are investigated with XRD measurements as shown in **Fig. 2a** and **Fig. S1**. With the exception of the three typical peaks owing to the Ni foam substrate and the reflections originated from the N-CNTs substrate, the identified diffraction peaks are indexed to the spinel $NiCo_2O_4$ structure (JCPDS: 73-1702). No impurity peaks are detected in the pattern, indicating the successful growth of $NiCo_2O_4$ nanosheets and the high phase purity of the as-synthesized samples. The spinel-related $NiCo_2O_4$ crystalline structure (space group *Fd3m*) in **Fig. 2b** shows that Ni atoms are embedded in the octahedron and the Co atoms are located in both the octahedral and tetrahedral sites, providing a 3D mesh of interstitial space for ion diffusion.[47] Moreover, the EDX spectrum demonstrates that the molar ratio between Ni and Co is almost 1:2 in agreement with the stoichiometric ratio of $NiCo_2O_4$. (**Fig. S2**)

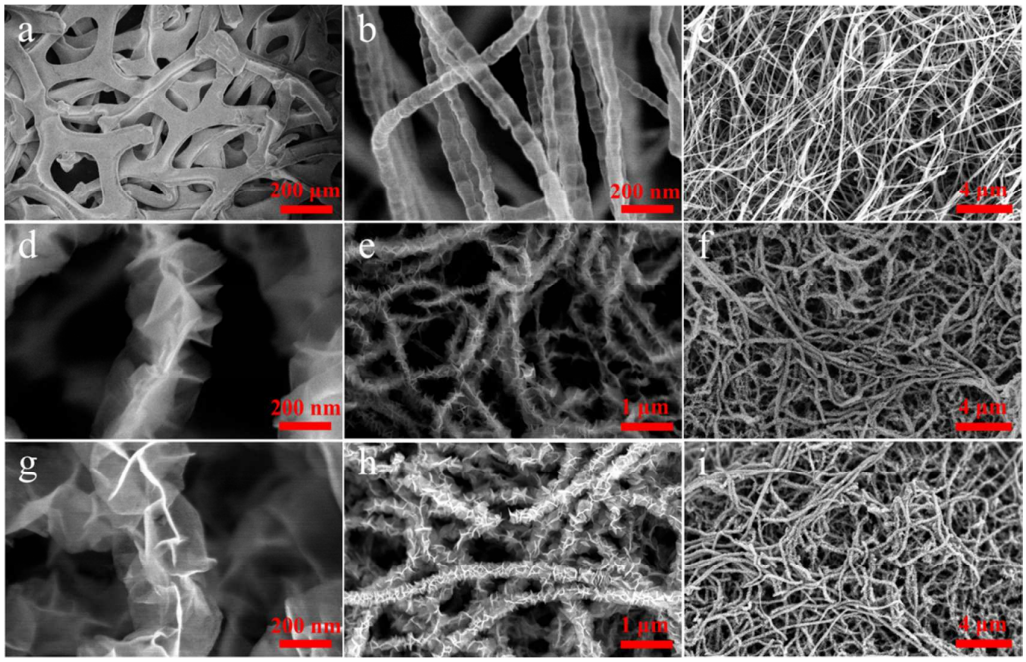

Fig. 3 SEM images of (a) pure Ni foam, (b, c) N-CNTs, (d, e, f) Ni foam/N-CNTs/ NiCo-precursor and (g, h, i) Ni foam/N-CNTs/ $NiCo_2O_4$ NS at different magnifications, respectively.

Fig. 3a shows that the original Ni foam has a smooth surface before N-CNTs growth. After CVD growth of N-CNTs, the surface of Ni foam becomes rough owing to a dense N-CNTs uniform mesh covering (**Fig. S3**). It can be seen from **Fig. 3b** that N-CNTs present a bamboo-like structure, indicating that nitrogen atoms were doped in the carbon nanotubes. This morphology revolution could be attributed to the shorter length of the C-N bond compared to the C-C bond, and this bond length change creates the curvature of the basal planes resulting in the bamboo-like structure.[43, 48] The diameter of the N-CNTs was around 60 nm, while the length could reach as long as tens of micrometers. More importantly, by entangling each other, the long and slim

N-CNTs are self-assembled into a 3D mesh network, which is in favor of active material electrodeposition onto the N-CNTs. Furthermore, the Ni foam/N-CNTs substrate exhibits a higher surface area of 6.94 $m^2 g^{-1}$ than the Ni foam of 0.89 $m^2 g^{-1}$. The surface area of N-CNTs was measured to be 77.29 $m^2 g^{-1}$ (**Fig. S4**). The high-magnification image (**Fig. 3d**) shows that the surface of the N-CNTs is wrapped by the thin NiCo-precursor nanosheets. The corresponding low-magnification images (**Fig. 3e** and **3f**) reveal that each N-CNT is homogeneously covered by the NiCo-precursor nanosheets. A large void space between the NiCo-precursor/N-CNTs still existed, which is advantageous for electrolyte penetration and fast ion and electron transportation. Remarkably, the ultrathin nanosheet structure is maintained after thermal treatment and there is no structural collapse or breakage in the as-prepared sample, demonstrating excellent structural stability (**Fig. 3g**, **3h** and **3i**). The SEM images of Ni foam/$NiCo_2O_4$ NS are show in **Fig. S5**. Although thin and dense layer of $NiCo_2O_4$ NS are uniformly covered on the surface of Ni foam, the thickness of nanosheets are thicker than that on N-CNTs due to the far lower surface area than the Ni foam/N-CNTs.

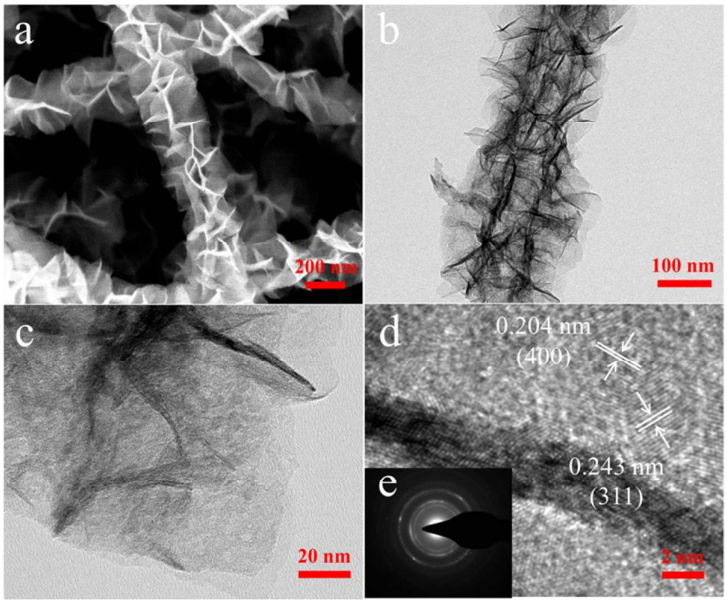

Fig. 4 (a) High-magnification SEM image and (b) TEM image of the N-CNTs/$NiCo_2O_4$ nanosheets. (c) TEM image and (d) high-magnification TEM image of the $NiCo_2O_4$ nanosheet (inset (e): SAED pattern of the nanosheets).

In order to further characterize the structure of the N-CNTs/$NiCo_2O_4$ composite, TEM was carried out by scratching the products down from the Ni foam. It can be clearly observed (**Fig. 4b)** that the crosslinked $NiCo_2O_4$ nanosheets' shells grow uniformly on the N-CNTs, forming a typical N-CNTs/ N-CNTs/$NiCo_2O_4$ core-shell architecture, in agreement with the SEM observation. The TEM images (**Fig. 4b** and **4c)** exhibit the fringes of N-CNTs and $NiCo_2O_4$ nanosheets, and further reveal that the ultrathin nanosheet morphology of the NiCo-precursor is well maintained after thermal treatment. The adjacent lattice fringes in **Fig. 4d** were determined to be 0.204 and 0.243 nm corresponding to the (400) and (311) lattice spaces of spinel $NiCo_2O_4$, respectively. The selected-area electron diffraction (SAED) pattern implies the

polycrystalline nature of the $NiCo_2O_4$ nanosheets (**Fig. 4e**).

Electrochemical measurement

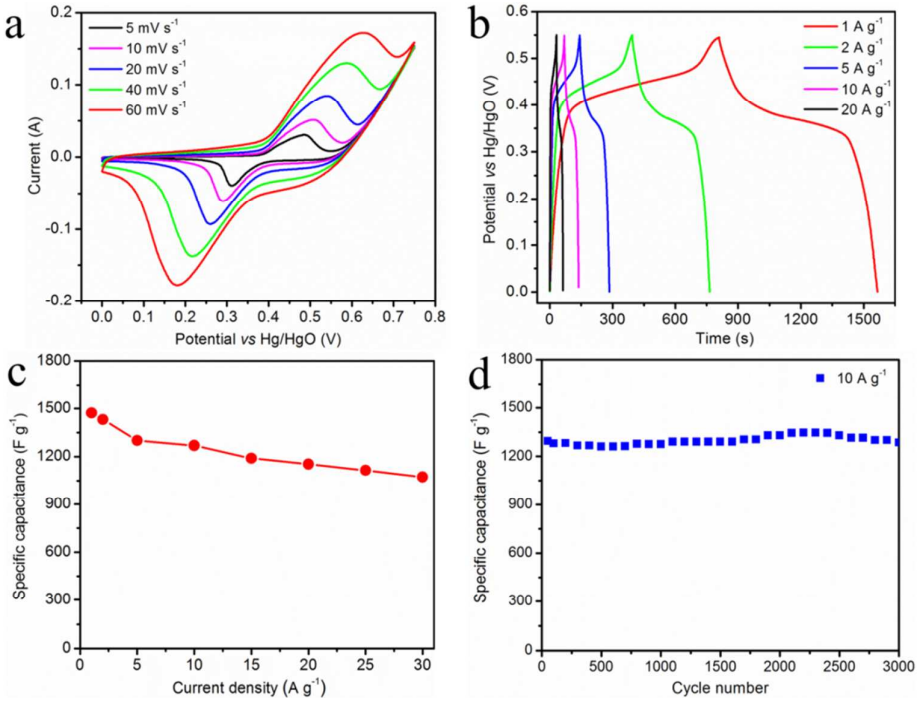

Fig. 5 Electrochemical characterizations of the 3D Ni foam/N-CNTs/$NiCo_2O_4$ NS electrode: (a) CV curves at various scan rates from 5 to 60 mV s^{-1}. (b) Charge and discharge curves at various current densities from 1 to 20 A g^{-1}. (c) Specific capacitances of the electrode as a function of current density. (d) The capacitance cycling performance at a current density of 10 A g^{-1}.

To evaluate the electrochemical performances of the binder-free Ni foam/N-CNTs/$NiCo_2O_4$ NS, the as-prepared products are fabricated as supercapacitor electrodes. In order to illustrate the N-CNTs superiority, the electrochemical properties of Ni foam/$NiCo_2O_4$ NS are measured under the same conditions (**Fig. S6**). **Fig. 5a** shows a comparison of the CV curves with various scan rates ranging from 5

to 60 mV s^{-1} in a potential window from 0 to 0.75 V *versus* Hg/HgO. Obviously, all the curves present a pair of oxidation and reduction peaks, which originate from the faradic redox reactions associated with M-O/M-O-OH, where M refers to Ni or Co.[12, 25] In addition, along with the increase of scan rates, the anodic/catholic peak shifts positively/negatively, respectively, a phenomenon which is ascribed to the electrode polarization at higher scan rates.[45, 49] Moreover, the linear plots of peak current is symmetric with the linear plots of the catholic peak current, indicating the 3D Ni foam/N-CNTs/$NiCo_2O_4$ NS composite possesses excellent reversibility.[50]

To further examine the charge storage capacity of our sample, galvanostatic charge–discharge (GCD) measurements were performed at various current densities, as shown in **Fig. 5b**. The obvious plateaus in the GCD curves verify the existence of faradaic processes, consistent with the CV results. The high symmetry of the GCD curves with small IR drop indicates a low internal resistance and an outstanding electrochemical reversibility of the 3D Ni foam/N-CNTs/$NiCo_2O_4$ NS. **Fig. S7** demonstrates that the Ni foam/N-CNTs makes little contribution to the total capacitance and thus can be ignored. Calculated from the discharge curves, the specific capacitances based on the mass of $NiCo_2O_4$ are 1472, 1431, 1300, 1269 and 1153 F g^{-1} at current densities of 1, 2, 5, 10 and 20 A g^{-1}, respectively. Furthermore, the rate capability is also excellent and only decreases 27% when the current density was increased from 1 to 30 A g^{-1} (**Fig. 5c**). The areal capacitance is 0.68 F/cm^2 at the current density of 1 mA cm^{-2}, and maintains 63% retention as the current density increased to 30 mA cm^{-2} (**Fig. S8**). However, the Ni foam/$NiCo_2O_4$ NS presents

relatively lower specific capacitance of 682 F g^{-1} and areal capacitance of 0.32 F/cm^2 at current densities of 1 A g^{-1} and 1 mA cm^{-2}, respectively (**Fig. S6**). In addition, the 3D Ni foam/N-CNTs/$NiCo_2O_4$ NS exhibits higher energy density and higher power density, as shown in the Ragone plot (**Fig. S9**). The energy density of Ni foam/N-CNTs/$NiCo_2O_4$ NS and Ni foam/$NiCo_2O_4$ NS reach 61.84 W h kg^{-1} and 28.65 W h kg^{-1} at a power density of 280 W kg^{-1} and maintain 45.04 and 21.50 W h kg^{-1} at a power density of 8251 W kg^{-1}, respectively.

The long-term cycling life of the 3D Ni foam/N-CNTs/$NiCo_2O_4$ NS composite electrode was evaluated by repeating the charging-discharging measurements at a high current density of 10 A g^{-1} (**Fig. 5d**). It is worth noting that after 3000 cycles, there is almost no decline in capacitance (more than 99% retention), indicating that the as-prepared electrode has a remarkable cycling stability. Even at a higher current density of 20 A g^{-1} with more cycling times (9000 cycles), the specific capacitances is still 960 F g^{-1}, corresponding to less than 19% loss of its original values (**Fig. 6a**). For Ni foam/$NiCo_2O_4$ NS electrode, the capacitance retention is 91.7% at a current density of 10 A g^{-1} (**Fig. 6f**). In general, the electrochemical performance of this as-prepared 3D Ni foam/N-CNTs/$NiCo_2O_4$ NS composite electrode is superior to other reported $NiCo_2O_4$-based ones, as shown in **Table 1**. The above results demonstrate that the binder-free Ni foam/N-CNTs/$NiCo_2O_4$ NS is an advanced electrode material for supercapacitor.

Table 1 Comparison of the electrochemical performances of the 3D Ni foam/N-CNTs/$NiCo_2O_4$ NS with other reported ones.

Nanostructures	Specific capacitance (F g^{-1})	Rate performance	Capacity retention	Refs
Ni foam/ N-CNTs/$NiCo_2O_4$ nanosheets	1472 (1 A g^{-1})	73% (30 A g^{-1})	99% (10 A g^{-1}, 3000 cycles) 81% (20 A g^{-1}, 9000 cycles)	This work
CNTs/$NiCo_2O_4$ core/shell	694 (1 A g^{-1})	82% (20 A g^{-1})	91% (4 A g^{-1}, 1500 cycles)	47
CNF/$NiCo_2O_4$ nanosheets	1002 (1 A g^{-1})	52% (20 A g^{-1})	93% (5 A g^{-1}, 2400 cycles)	51
Ni/$NiCo_2O_4$ nanosheets	899 (1 A g^{-1})	68% (20 A g^{-1})	85% (5 A g^{-1}, 6000 cycles)	10
Ni foam/$NiCo_2O_4$ nanosheets	895 (1 A g^{-1})	73% (20 A g^{-1})	73% (5 A g^{-1}, 2000 cycles)	40
$NiCo_2O_4$ @graphene	778 (1 A g^{-1})	71% (20 A g^{-1})	90% (10 A g^{-1}, 10000 cycles)	52
$NiCo_2O_4$@ $Co_{0.33}Ni_{0.67}(OH)_2$ core/shell	1045 (1 A g^{-1})	84% (50 A g^{-1})	80% (5 A g^{-1}, 3000 cycles)	22

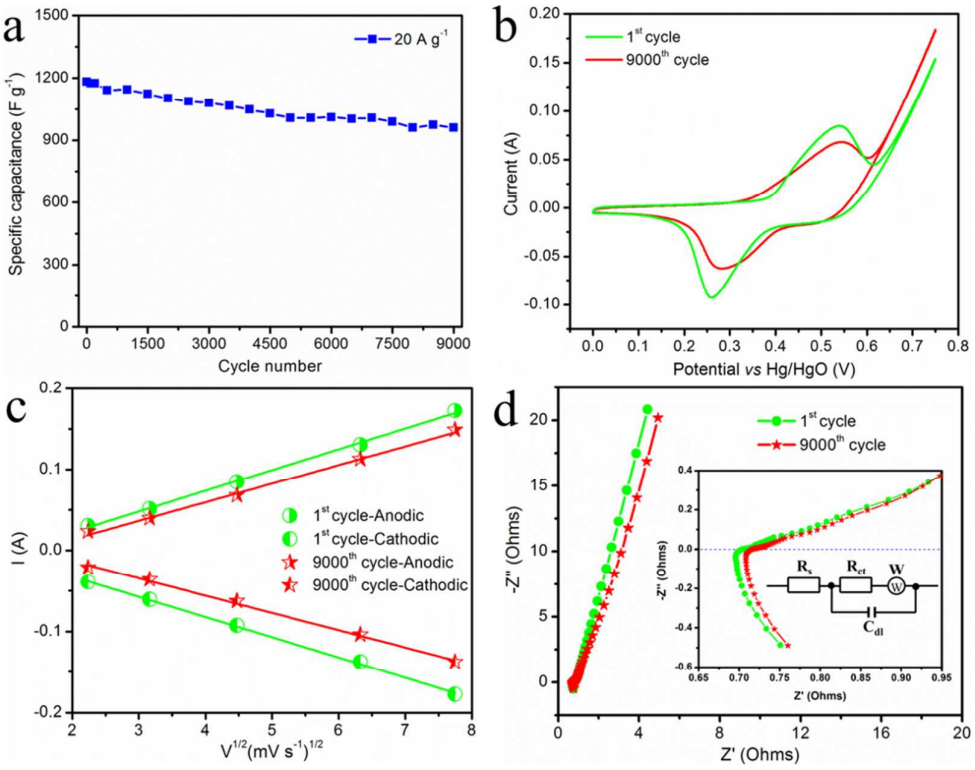

Fig. 6 Electrochemical characterizations of the 3D Ni foam/N-CNTs/$NiCo_2O_4$ NS electrode: (a) Cycling performance at a high current density of 20 A g^{-1}. (b) CV curves of the 1st and 9000th cycle at a scan rate of 20 mV s^{-1}. (c) The linear plots of anodic and cathodic peak currents versus the square root of the scan rates of the 1st and 9000th cycle. (d) Nyquist curve of the 1st and 9000th cycle of the electrode. The inset is the enlarged plots of the high frequency region.

The corresponding CV curves of the electrode at the 1st and 9000th cycle at a scan rate of 20 mV s^{-1} are demonstrated in **Fig. 6b**. The CV area of the 9000th cycle is slightly smaller than that of the 1st cycle, indicating a minor decrease in specific capacitance, in agreement with the result shown in the long charge/discharge cycling test. Even after 9000 cycles at a high current density of 20 A g^{-1}, the CV curves still

present an obvious pair of oxidation and reduction peaks (**Fig. S10**). Moreover, a good linear dependence of anodic and catholic peak currents at different scan rates *vs* the square root of scan rates is shown in **Fig. 6c**, revealing that the diffusion of OH- is a controlled process.[53] Meanwhile, the linear plots of the anode peak current is symmetrical with the linear plots of the catholic peak current, indicating the as-prepared products own excellent reversibility. Compared to the linear responses of the graphs, the linear plots of the peak current of the 1st cycle presents a steeper slope than that of the 9000th cycle, suggesting faster protons diffusion at the initial cycle. EIS analysis was further adopted to investigate the change of the as-prepared products from 1st to 9000th cycle (**Fig. 6d**). Both impedance spectra display a linear region in the low-frequency range, which corresponds to the diffusive resistance (Warburg impedance). It can be found that the Warburg impedance is slightly increased after 9000 cycles. Meanwhile, in the high-frequency region, the solution resistance after 9000 cycles is slightly bigger than that of the 1st cycle, revealing a decrease tendency of the electron conductivity of the 3D Ni foam/N-CNTs/$NiCo_2O_4$ NS electrode.[18, 53] The EIS analysis is in agreement with that the special capacitance decreased after 9000 cycles at a high current density of 20 A g^{-1}.

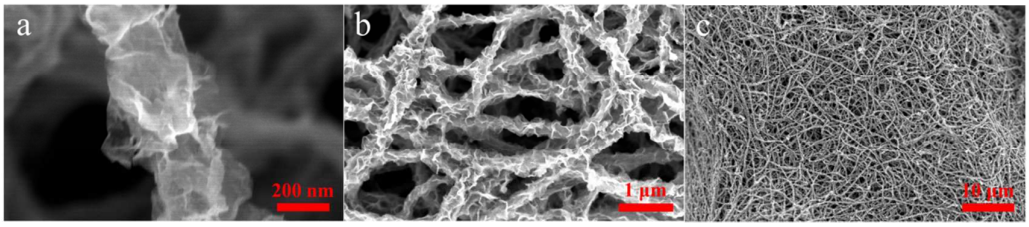

Fig. 7 (a,b,c) Low- and high-magnification SEM images of the 3D Ni foam/N-CNTs/$NiCo_2O_4$ NS electrode after 9000 cycles at a high current density of 20

A g^{-1}.

Fig. 7 reveals the SEM images of the 3D Ni foam/N-CNTs/$NiCo_2O_4$ NS after 9000 cycles at a high current density of 20 A g^{-1}. From the high-magnification SEM image, it can be clearly seen that the morphology of the thin nanosheets is well maintained, except for a slight roughness on the surface (**Fig. 7a**). Furthermore, the 3D network of N-CNTs/$NiCo_2O_4$ NS is also retained and there is no structural collapse or aggregation, demonstrating excellent structural stability (**Fig. 7b** and **7c**).

To explain the remarkable electrochemical performance of the 3D Ni foam/N-CNTs/$NiCo_2O_4$ NS electrode, including high special capacitance, superior rate capability and long cycle life, we can elaborate from the following merits: (1) the 3D conducting network of N-CNTs not only offers a strong skeleton for homogeneous electrodeposition of $NiCo_2O_4$ NS, but also provides a good electrical conducting pathway for ion and electron transportation and redox kinetics of $NiCo_2O_4$ NS; (2) the large void space between N-CNTs/$NiCo_2O_4$ NS allows electrolyte to easily penetrate into the inner-space and can endure the volume change during electrochemical measurement; (3) the direct electrodeposition of $NiCo_2O_4$ NS on N-CNTs could ensure good mechanical adhesion and decrease the contact resistance between the $NiCo_2O_4$ NS and the current collectors; (4) the ultrathin and interconnected nanostructure of $NiCo_2O_4$ NS possess numerous active sites for the redox reaction and provides a short diffusion path for fast ion transport. (5) the high conductive N-CNTs directly grown on the Ni foam current collector benefits the fast electron transfer and

avoids the use of polymer binder and conductive additives. Therefore, these intriguing advantages undoubtedly account for the excellent electrochemical performance of the 3D Ni foam/N-CNTs/$NiCo_2O_4$ NS electrode.

Conclusion

In summary, we have fabricated a 3D Ni foam/N-CNTs/$NiCo_2O_4$ NS electrode by combining a CVD method and a simple electrochemical deposition method in combination with a calcination process. The as-obtained sample is directly used as a binder-free electrode for supercapacitors, which possesses remarkable electrochemical performance. The 3D Ni foam/N-CNTs/$NiCo_2O_4$ NS electrode exhibits a high specific capacitance of 1472 F g^{-1} at the current density of 1 A g^{-1}, a remarkable rate capability (73% retention as the current density increased to 30 A g^{-1}) and excellent cycling stability (99% retention over 3000 cycles at the current density of 10 A g^{-1} and 81% retention after 9000 cycles at the current density of 20 A g^{-1}). The outstanding supercapacitive performance is attributed to the 3D conducting network of N-CNTs, the binder-free design of this electrode, the large open spaces between N-CNTs/$NiCo_2O_4$ NS and the ultrathin and interconnected NS structure. These merits offer a strong skeleton for homogeneous electrodeposition, endure the volume change, provide a good electrical conducting pathway for the transportation of both ion and electron, allow electrolyte to easily penetrate into the inner-space, and provide many active sites and short diffusion path. Therefore, the 3D Ni foam/N-CNTs-based

network as a novel substrate can compound with other electrode materials for supercapacitors and other energy-storage devices.

Acknowledgments

We thank the National High Technology Research and Development Program of China (863Program) (2013AA050905), the National Natural Science Foundation of China (No.51222212), the financial support of LPMT, CAEP (ZZ13007 and ZZ14004), Project 2013A030214 supported by CAEP, the Science and Technology Foundation of China Academy of Engineering Physics (No. 2012B0302041) for their financial support. We are grateful to Margaret Yau for their valuable discussions and assistance in measurements.

References

1. S. Chu and A. Majumdar, *Nature*, 2012, **488**, 294-303.

2. J. Jiang, Y. Y. Li, J. P. Liu, X. T. Huang, C. Z. Yuan and X. W. Lou, *Adv. Mater.*, 2012, **24**, 5166-5180.

3. J. R. Miller and P. Simon, *Science*, 2008, **321**, 651-652.

4. P. Simon and Y. Gogotsi, *Nat. Mater.*, 2008, **7**, 845-854.

5. V. Augustyn, P. Simon and B. Dunn, *Energy Environ. Sci.*, 2014, **7**, 1597-1614.

6. J. Yan, Q. Wang, T. Wei and Z. J. Fan, *Adv. Energy Mater.*, 2014, **4**, 130016-1300859.

7. R. Yi, S. R. Chen, J. X. Song, M. L. Gordin, A. Manivannan and D. H. Wang, *Adv. Funct. Mater.*, 2014, **24**, 7433-7439.

8. P. Simon and Y. Gogotsi, *Acc. Chem. Res.*, 2013, **46**, 1094-1103.

9. X. H. Xia, J. P. Tu, Y. Q. Zhang, X. L. Wang, C. D. Gu, X. B. Zhao and H. J. Fan, *ACS Nano*, 2012, **6**, 5531-5538.

10. G. X. Gao, H. B. Wu, S. J. Ding, L. M. Liu and X. W. Lou, *Small*, 2014, **11**, 804-808.

11. X. H. Xia, Y. Q. Zhang, D. L. Chao, C. Guan, Y. J. Zhang, L. Li, X. Ge, I. M. Bacho, J. P. Tu and H. J. Fan, *Nanoscale*, 2014, **6**, 5008-5048.

12. G. Q. Zhang, H. B. Wu, H. E. Hoster, M. B. Chan-Park and X. W. Lou, *Energy Environ. Sci.*, 2012, **5**, 9453-9456.

13. K. K. Lee, W. S. Chin and C. H. Sow, *J. Mater. Chem. A*, 2014, **2**, 17212-17248.

14. J. Wu, R. Mi, S. M. Li, P. Guo, J. Mei, H. Liu, W. M. Lau and L. M. Liu, *RSC Adv.*, 2015, **5**, 25304-25311.

15. C. H. An, Y. J. Wang, Y. N. Huang, Y. N. Xu, C. C. Xu, L. F. Jiao and H. T. Yuan, *CrystEngComm*, 2014, **16**, 385-392.

16. X. C. Dong, Y. F. Zhang, M. Z. Mingze, Y. Jun, H. Q. Su, W. Huang and X. C. Dong, *Nanoscale*, 2014, **6**, 4303-4308.

17. J. W. Xiao and S. H. Yang, *RSC Adv.*, 2011, **1**, 588-595.

18. J. Du, G. Zhou, H. M. Zhang, C. Cheng, J. M. Ma, W. F. Wei, L. B. Chen and T. H. Wang, *ACS Appl. Mater. Interfaces*, 2013, **5**, 7405-7409.

19. X. Y. Liu, S. J. Shi, Q. Q. Xiong, L. Li, Y. J. Zhang, H. Tang, C. D. Gu, X. L. Wang and J. P. Tu, *ACS Appl. Mater. Interfaces*, 2013, **5**, 8790-8795.

20. H. Xia, C. Y. Hong, B. Li, B. Zhao, Z. X. Lin, M. B. Zheng, S. V. Savilov and S. M. Aldoshin, *Adv. Funct. Mater.*, 2015, **25**, 627-635.

21. G. Q. Zhang and X. W. Lou, *Adv. Mater.*, 2013, **25**, 976-979.

22. K. B. Xu, R. J. Zou, W. Y. Li, Q. Liu, X. J. Liu, L. An and J. Q. Hu, *J. Mater. Chem. A*, 2014, **2**, 10090-10097.

23. L. Yu, G. Q. Zhang, C. Z. Yuan and X. W. Lou, *Chem. Commun.*, 2013, **49**, 137-139.

24. H. Xia, D. D. Zhu, Z. T. Luo, Y. Yu, X. Q. Shi, G. L. Yuan and J. P. Xie, *Sci. Rep.*, 2013, **3**, 2978-2985.

25. L. Huang, D. C. Chen, Y. Ding, S. Feng, Z. L. Wang and M. L. Liu, *Nano Lett.*, 2013, **13**, 3135-3139.

26. L. F. Chen, X. D. Zhang, H. W. Liang, M. G. Kong, Q. F. Guan, P. Chen, Z. Y. Wu and S. H. Yu, *ACS Nano*, 2012, **6**, 7092-7102.

27. Y. Zhao, R. Nakamura, K. Kamiya, S. Nakanishi and K. Hashimoto, *Nat. Comm.*, 2013, **4**, 2390-2397.

28. Y. Wang, Y. Y. Shao, D. W. Matson, J. H. Li and Y. H. Lin, *ACS Nano*, 2010, **4**, 1790-1798.

29. X. C. Liu, S. M. Li, J. Mei, W. M. Lau, R. Mi, Y. C. Li, H. Liu and L. M. Liu, *J. Mater. Chem. A*, 2014, **2**, 14429-14438.

30. J. X. Song, T. Xu, M. L. Gordin, P. Y. Zhu, D. P. Lv, Y. B. Jiang, Y. S. Chen, Y. H. Duan and D. H. Wang, *Adv. Funct. Mater.*, 2014, **24**, 1243-1250.

31. Q. Tang, Z. Zhou and Z. F. Chen, *Nanoscale*, 2013, **5**, 4541-4583.

32. P. Y. Zhu, J. X. Song, D. P. Lv, D. H. Wang, C. Jaye, D. A. Fischer, T. P. Wu and Y. S. Chen, *J. Phys. Chem. C*, 2014, **118**, 7765-7771.

33. Y. Y. Shao, S. Zhang, M. H. Engelhard, G. S. Li, G. C. Shao, Y. Wang, J. Liu, I. A. Aksay and Y. H. Lin, *J. Mater. Chem.*, 2010, **20**, 7491-7496.

34. Z. S. Wu, W. C. Ren, L. Xu, F. Li and H. M. Cheng, *ACS Nano*, 2011, **5**, 5463-5471.

35. H. Abou-Rachid, A. Hu, V. Timoshevskii, Y. F. Song and L. S. Lussier, *Phys. Rev. Lett.*, 2008, **100**, 196401-19604.

36. K. P. Gong, F. Du, Z. H. Xia, M. Durstock and L. M. Dai, *Science*, 2009, **323**, 760-764.

37. G. Q. Jian, Y. Zhao, Q. Wu, L. J. Yang, X. Z. Wang and Z. Hu, *J. Phys. Chem. C*, 2013, **117**, 7811-7817.

38. H. Zhang, X. J. Liu, R. L. Wang, R. Mi, S. M. Li, Y. H. Cui, Y. F. Deng, J. Mei and H. Liu, *J. Power Sources*, 2015, **274**, 1063-1069.

39. J. Wang, L. F. Shen, P. Nie, X. L. Yun, Y. L. Xu, H. Dou and X. G.

Zhang, *J. Mater. Chem. A*, 2015, **3**, 2853-2860.

40. W. W. Zhou, D. Z. Kong, X. T. Jia, C. Y. Ding, C. N. Cheng and G. W. Wen, *J. Mater. Chem. A*, 2014, **2**, 6310-6315.

41. C. Z. Yuan, J. Y. Li, L. R. Hou, X. G. Zhang, L. F. Shen and X. W. Lou, *Adv. Funct. Mater.*, 2012, **22**, 4592-4597.

42. F. Li, Y. Xing, M. Huang, K. L. Li, T. T. Yu, Y. X. Zhang and D. Losic, *J. Mater. Chem. A*, 2015, **3**, 7855-7861.

43. H. Liu, Y. Zhang, R. Y. Li, X. L. Sun, S. Désilets, H. Abou-Rachid, M. Jaidann and L. S. Lussier, *Carbon*, 2010, **48**, 1498-1507.

44. R. Mi, S. M. Li, X. C. Liu, L. M. Liu, Y. C. Li, J. Mei, Y. G. Chen, H. Liu, H. Wang, H. Yan and W. M. Lau, *J. Mater. Chem. A*, 2014, **2**, 18746-18753.

45. W. W. Liu, C. X. Lu, X. L. Wang, K. Liang and B. K. Tay, *J. Mater. Chem. A*, 2015, **3**, 624-633.

46. Q. F. Wang, X. F. Wang, B. Liu, G. Yu, X. J. Hou, D. Chen and G. Z. Shen, *J. Mater. Chem. A*, 2013, **1**, 2468-2473.

47. W. W. Liu, C. X. Lu, K. Liang and B. K. Tay, *J. Mater. Chem. A*, 2014, **2**, 5100-5107.

48. P. Ayala, A. Grüneis, T. Gemming, D. Grimm, C. Kramberger, M. H. Rümmeli, F. L. Freire, H. Kuzmany, R. Pfeiffer, A. Barreiro, B. Büchner and T. Pichler, *J. Phys. Chem. C*, 2007, **111**, 2879-2884.

49. D. P. Cai, B. Liu, D. D. Wang, L. L. Wang, Y. Liu, H. Li, Y. R.

Wang, Q. H. Li and T. H. Wang, *J. Mater. Chem. A*, 2014, **2**, 4954-4960.

50. Y. Qian, R. Liu, Q. F. Wang, J. Xu, D. Chen and G. Z. Shen, *J. Mater. Chem. A*, 2014, **2**, 10917-10922.

51. G. Zhang and X. W. Lou, *Sci. Rep.*, 2013, **3**, 1470-1475.

52. Y. Y. Wei, S. Q. Chen, D. W. Su, B. Sun, J. G. Zhu and G. X. Wang, *J. Mater. Chem. A*, 2014, **2**, 8103-8109.

53. Y. J. Chen, B. H. Qu, L. Q. Hu, Z. Xu, Q. H. Li and T. H. Wang, *Nanoscale*, 2013, **5**, 9812-9820.

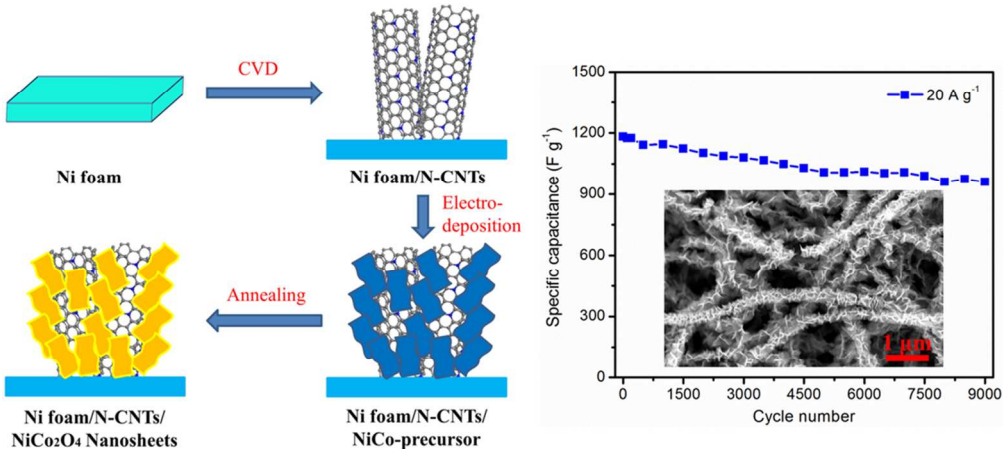

A novel three-dimensional (3D) Ni foam/N-CNTs/NiCo2O4 nanosheets electrode was synthesized by combining a chemical vapor deposition method and a facile electrochemical deposition method followed by a calcination process, and exhibits superior supercapacitive performances with high specific capacitance (1472 F g-1 at 1 A g-1), remarkable rate capability and excellent cycling stability (less than 1% loss after 3000 cycles).
101x45mm (300 x 300 DPI)